INTERNATIONAL JOURNAL FOR NUMERICAL METHODS IN ENGINEERING
Int. J. Numer. Meth. Engng (2009)
Published online in Wiley InterScience (www.interscience.wiley.com). DOI: 10.1002/nme.2551

Uncertainty quantification in chemical systems

H. N. Najm[1,*,†], B. J. Debusschere[1], Y. M. Marzouk[1], S. Widmer[1] and O. P. Le Maître[2]

[1]*Sandia National Laboratories, P. O. Box 969, MS 9051, Livermore, CA 94551, U.S.A.*
[2]*LIMSI-CNRS, BP 133, F91-403 Orsay, France*

SUMMARY

We demonstrate the use of multiwavelet spectral polynomial chaos techniques for uncertainty quantification in non-isothermal ignition of a methane–air system. We employ Bayesian inference for identifying the probabilistic representation of the uncertain parameters and propagate this uncertainty through the ignition process. We analyze the time evolution of moments and probability density functions of the solution. We also examine the role and significance of dependence among the uncertain parameters. We finish with a discussion of the role of non-linearity and the performance of the algorithm. Copyright © 2009 John Wiley & Sons, Ltd.

Received 30 June 2008; Accepted 1 December 2008

KEY WORDS: uncertainty quantification; polynomial chaos; multiwavelet; chemistry; ignition

1. INTRODUCTION

Uncertainty quantification (UQ) is a pre-requisite for truly predictive computations of physical models, enabling assignment of confidence in model predictions. This is particularly true for models involving significant uncertainty in model structure, parameters, geometry, inputs, initial and/or boundary conditions. It is also especially true for models with strong non-linearities that can amplify relatively small parametric uncertainties, leading to large uncertainties in predictions. These qualities are very much present in chemical systems. Detailed chemical kinetic models typically involve a large number of uncertain parameters, including reaction rate constants and

*Correspondence to: H. N. Najm, Sandia National Laboratories, P. O. Box 969, MS 9051, Livermore, CA 94551, U.S.A.
†E-mail: hnnajm@sandia.gov

Contract/grant sponsor: US Department of Energy (DOE); contract/grant number: DE-AC04-94-AL85000
Contract/grant sponsor: Office of Basic Energy Sciences
Contract/grant sponsor: Division of Chemical Sciences, Geosciences, and Biosciences

thermodynamic parameters, many of which are poorly known. They also involve strong non-linear dependence on temperature, through high activation energy Arrhenius reaction rate exponentials.

Under conditions where uncertainties are small, UQ methods based on sensitivity analysis [1–3] and variance propagation [1, 4–6] have been used effectively. When larger uncertainties are present, local sensitivity methods are not adequate. In this context, probabilistic methods provide a more accurate means of UQ, presuming sufficient information for probabilistic characterization of relevant uncertain parameters. Recent years have seen a significant development in the use of spectral polynomial chaos (PC) [7–12] techniques for probabilistic UQ. Ghanem and Spanos [13] provided the first demonstration for the use of PC expansions (PCEs) for the representation of random variables (RVs) for probabilistic UQ in computational models. This methodology has been successfully used for UQ in a variety of physical systems [14–22]. Investigations have employed both sampling-based 'non-intrusive' collocation methods [17, 23, 24] where relevant Galerkin projections are computed numerically, and 'intrusive' methods involving Galerkin projection reformulation of governing equations [13]. The original PC formulation of Wiener [7] is a spectral expansion in terms of Hermite polynomial functionals of Gaussian RVs. Where necessary, we refer to this construction specifically as the Wiener–Hermite (WH) PC. This construction was extended to a generalized polynomial chaos (GPC) representation [25], employing a range of orthogonal polynomials in the Askey scheme [26, 27], coupled with associated RV bases. GPC constructions have been used successfully in various physical systems [25, 28, 29]. PC methods have also been extended to employ local expansions in terms of compact-support bases on block-decomposed stochastic spaces [30–33]. These constructions have proven most effective for dealing with strong non-linearities and bifurcations. Other local constructions have also been developed, employing Lagrange interpolants [34–41].

There have been numerous applications of UQ in the context of chemical systems, employing various methodologies. Turanyi *et al.* [6] used sensitivity information coupled with variance propagation [4] for UQ in computations of a methane flame. Phenix *et al.* [42] used a collocation-based PC method [43, 44], where PCE modes of model outputs are found by solving an algebraic equation system, and applied it in the context of a super-critical water oxidation reactor. Reagan *et al.* [24] used non-intrusive PC UQ, employing Latin Hypercube sampling, applied to the same H_2–O_2 system of [42], for ignition and one-dimensional flame studies. Extraction of sensitivity information from PC UQ results in this system was outlined in [45]. Further, Reagan *et al.* [46] presented an intrusive reformulation of the governing equations of a chemical system using global WH PC. They illustrated the challenges with this system, particularly the need for high order for stability, although no specific finite order was found to be satisfactory. This challenge with the handling of chemical systems using global PC led to the development of local multiwavelet PC UQ methods by Le Maître *et al.* [30, 31] and their application to isothermal ignition [32].

The present work explores the first utilization of the intrusive multiwavelet PC UQ method [32] in the context of non-isothermal ignition of a hydrocarbon chemical system. The role of temperature is key in many chemical systems of practical interest in combustion. Particularly, the non-linearity of the Arrhenius chemical source term, as exhibited by both the pre-exponential constant and the activation energy exponential, presents significant challenges to efficient and robust PC UQ computations. We also address the evaluation of a probabilistic representation of uncertain chemical model parameters from data, with particular emphasis on the exploration and use of inherent *correlation*, and associated linear dependence, between the parameters. While the importance of such correlations has been highlighted in sensitivity and variance propagation uncertainty studies in chemical models [4], their relevance has not been addressed in hitherto

DOI: 10.1002/nme

full probabilistic UQ studies in these systems. We highlight the crucial need for using the true dependence relationships among the parameters for accurate estimation of uncertainty in chemical model predictions.

In the following, we begin by a discussion of inference of Arrhenius model parameters from data. We then proceed to the forward propagation of uncertainty in a chemical model. We briefly outline the basics of PC and the multiwavelet construction, before describing the Galerkin reformulation of the governing equations of the present chemical system. This is followed by a demonstration of the method in the context of methane–air ignition, and a discussion of the results, examining the time evolution of the uncertain solution and the key role of dependence relationships among the parameters. We finish with a discussion of the performance of the scheme in the context of strong non-linearity.

2. INFERENCE OF UNCERTAIN ARRHENIUS PARAMETERS

We focus on the ignition of a stoichiometric methane–air mixture under constant atmospheric pressure. An accurate description of methane–air chemistry requires a detailed chemical kinetic model accounting for all relevant elementary reaction steps and intermediates, typically involving more than 50 chemical species and hundreds of reactions. For the present purpose of demonstrating UQ in non-isothermal ignition, we employ a global single-step irreversible reaction model for simplicity. While this model excludes any realistic chemical details, it retains the fast time scale and strong non-linearity of ignition with suitable choices of the global reaction rate parameter constants.

We begin by calibrating the global model parameters using the detailed GRImech3.0 [47] chemical kinetic model for methane–air. We solve the ignition problem using the detailed chemistry model, starting from the same initial condition that will be used for the global model solution, providing what, for the present purposes, is the 'exact' solution to the problem.

In a practical setting, where reaction rate parameters are found empirically from experimental observations, the resulting uncertainty in the inferred parameters reflects the noise and sparsity of the data, as well as the model structure. In the present context, we seek to infer global model parameters with meaningful uncertainty, i.e. with uncertainty that does reflect model structure and some presumed noisy data. We define the 'data' to be the CH_4 mass fraction solution found using the detailed GRImech3.0 model, with added Gaussian noise to represent experimental instrument noise. The number of data points, and the amplitude of added noise, is chosen to arrive at a measure of uncertainty in the inferred global model parameters. The purpose of this exercise is to examine the structure of the joint probability density function (PDF) that might be observed among these parameters from an actual experiment and to proceed with the forward UQ problem using such a PDF structure.

The single-step global irreversible reaction is simply written as

$$CH_4 + 2O_2 \rightarrow CO_2 + 2H_2O \tag{1}$$

If this were an elementary forward reaction, its rate of progress would be given by the product of the reactants concentrations, each raised to its stoichiometric coefficient, multiplied by the temperature-dependent forward reaction rate $k_f(T)$, given by an Arrhenius expression

$$k_f(T) = AT^n e^{-E/R^0 T} \tag{2}$$

DOI: 10.1002/nme

where A is the pre-exponential Arrhenius rate constant, n is the temperature exponent, E is the activation energy, and $R^0 = 1.98598\,\mathrm{cal/mol\,K}$ is the universal gas constant. In the context of a global rate expression, the rate of progress, $\mathscr{R}$, may be generally written as

$$\mathscr{R} = [CH_4]^x [O_2]^y k_f(T) \quad (\mathrm{mol/cm^3 \cdot s}) \tag{3}$$

where $[\cdot]$ denotes concentration ($\mathrm{mol/cm^3}$). The Arrhenius parameters, as well as the concentration powers (x, y), are generally found by fitting to data or more detailed models [48, 49]. In the following, with no loss of generality, we presume $n = 0$ and $(x, y) = (1, 1)$, such that the pair of parameters (A, E) are the key objects of inference.

Further, we presume a measurement model with Gaussian noise whose variance is proportional to the signal amplitude. We represent the instrument noise as $\varepsilon \sim N(0, \sigma^2)$, with a variance given by

$$\sigma^2 = p + q Y^d_{CH_4} \tag{4}$$

where $p, q > 0$ are characteristic of the experiment and $Y^d_{CH_4}$ is the detailed chemistry computed CH_4 mass fraction. With stoichiometric initial conditions, and an initial temperature of 1050 K, the time evolution of $Y^d_{CH_4}$, as well as the selected data points with added noise, is shown in Figure 1. The noisy data is generated presuming $\ln p = -14$, $\ln q = -10$, in the noise model, such that a 6σ noise amplitude of $\sim 20\%$ is observed at the initial high value of $Y^d_{CH_4}$. With this initial temperature, and a stoichiometric mixture, ignition occurs in ~ 0.5 s, as shown in Figure 1.

With given noisy measurements of $Y_{CH_4}(t)$ over a range of time, best-fit values of A and E can be inferred using a suitable regression procedure. In order to infer probabilistic representations of the parameters, i.e. a joint PDF that describes their marginal distributions and correlations, we resort to a Bayesian parameter estimation strategy [50–52]. We define the inference problem on a four-dimensional parametric space, namely $(\ln A, \ln E, \ln p, \ln q)$, where the noise model

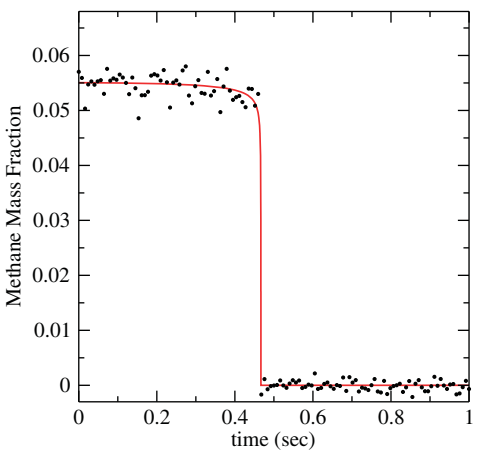

Figure 1. Decay of the mass fraction of methane during ignition of a stoichiometric methane–air mixture. The solid line is the detailed-chemistry solution found using GRImech3.0. The symbols are the 'data' points chosen at fixed time intervals from the detailed solution, and with added Gaussian random noise, to simulate experimental measurement noise.

DOI: 10.1002/nme

parameters are treated as hyperparameters to be inferred along with the main parameters of interest $(\ln A, \ln E)$. Bayes theorem is written as follows for this system [50]

$$p(\mathscr{P}|\mathfrak{D}) \propto p(\mathfrak{D}|\mathscr{P})\pi(\mathscr{P}) \tag{5}$$

where $\mathscr{P} = (\ln A, \ln E, \ln p, \ln q)$ is the parameter vector, $p(\mathscr{P}|\mathfrak{D})$ is the sought-after 'posterior' distribution, i.e. the joint PDF over the parameters given the data, $p(\mathfrak{D}|\mathscr{P})$ is the likelihood function determined from the forward model of the system with the above noise model, and $\pi(\mathscr{P})$ is the prior, encapsulating known information about the parameters prior to observation of data. We use uniform priors for all four parameters.

The posterior distribution can be explored using a Metropolis–Hastings Markov Chain Monte Carlo (MCMC) procedure [50, 53–55]. Conventional MCMC employs a fixed pre-specified 'proposal' distribution at each step of the chain. Depending on the unknown structure of the posterior, the proposal distribution can have a significant impact on the convergence rate of the MCMC procedure. This was indeed the case in the present work, where very poor 'mixing', and therefore convergence, was observed with the conventional procedure. As a result, it was necessary to resort to an *adaptive* MCMC procedure [56, 57] to ensure accurate and efficient exploration of the posterior distribution. The adaptive algorithm discovers the covariance structure of the posterior and uses it, with an adaptively optimized scale factor, as the MCMC proposal distribution. The scale factor is optimized to achieve an acceptance probability of 0.2. The adaptive algorithm is ergodic, retaining convergence of the Markov chain to the stationary posterior distribution.

We choose starting conditions for the MCMC chain near the expected solution from the simulated data and run a sufficiently long chain to explore the posterior. The extent of 'good' mixing in the chain is illustrated in Figure 2, where successive samples of the four parameters are shown over a 10 K long segment of the chain. This degree of mixing is observed consistently after the first 5–10 K samples. Statistics are drawn from a roughly 2×10^6 long chain.

The resulting marginal PDFs for $\ln A$ and $\ln E$ are shown in Figure 3, indicating nearly Gaussian statistics, with means of $\mu_{\ln A} = 34.10316$ and $\mu_{\ln E} = 10.817866$; and standard deviations of $\sigma_{\ln A} = 2.28 \times 10^{-3}$ and $\sigma_{\ln E} = 6.86 \times 10^{-5}$. The joint marginal PDF of $(\ln A, \ln E)$, $p(\ln A, \ln E|\mathfrak{D})$,

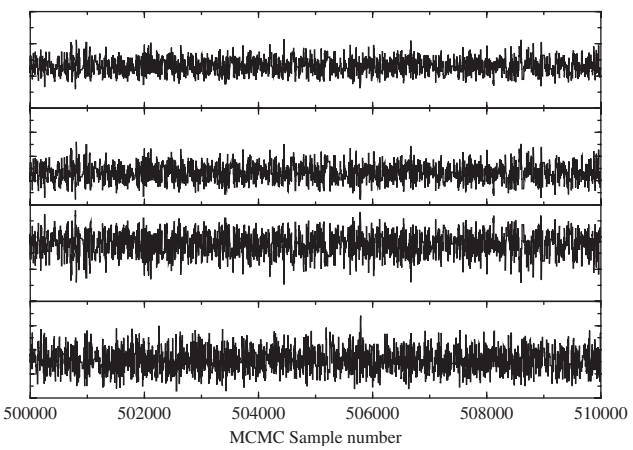

Figure 2. MCMC sampling during a 10 K number of samples, illustrating the degree of mixing in the chain among the four parameters, arranged as $(\ln A, \ln E, \ln p, \ln q)$ from the top down.

DOI: 10.1002/nme

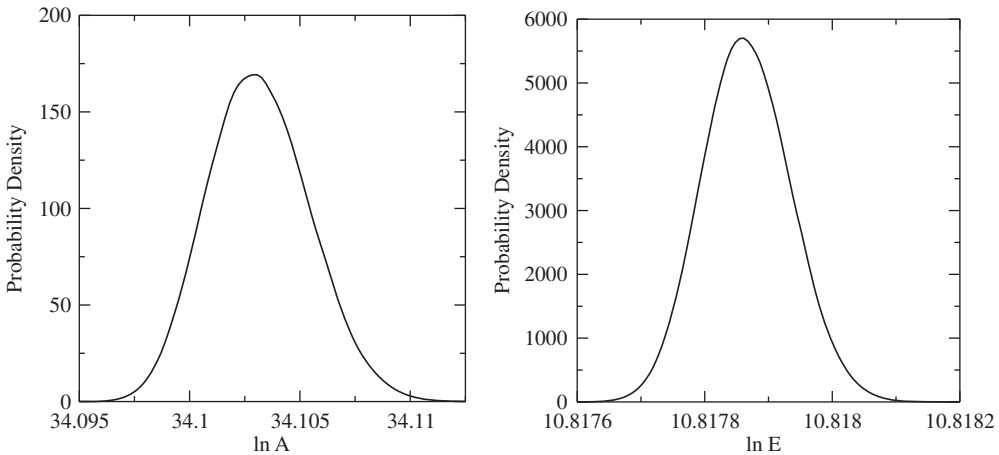

Figure 3. Marginal PDFs of $\ln A$ and $\ln E$ found using the Bayesian analysis.

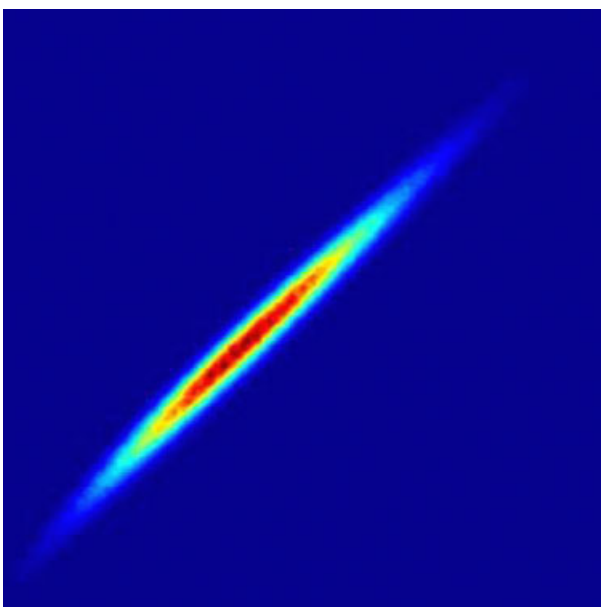

Figure 4. Joint marginal PDF of $(\ln A, \ln E)$ found using the Bayesian analysis.

exhibits a narrow ridge along a straight line in the $(\ln A, \ln E)$ plane, as can be seen in Figure 4. This PDF structure suggests a high degree of correlation between the two parameters, and therefore a degree of linear dependence between them. This dependence is inherent in the forward model and the physics of the system: the higher the pre-exponential constant A, the larger the activation energy E must be to remain consistent with the data. The posterior PDF is quite narrow, even with the high degree of noise evident in Figure 1. This long narrow ridge led to the convergence challenges

DOI: 10.1002/nme

with the conventional non-adaptive MCMC procedure. The adaptive procedure performs well by learning and using a proposal distribution with the same covariance structure as the posterior PDF. On the other hand, the strong correlation, and evidence for linear dependence between $\ln A$ and $\ln E$, serves to, in fact, simplify the forward UQ problem in the present context. It is a reasonable approximation to presume a perfect correlation and employ a single stochastic degree of freedom to represent uncertainty in both $\ln A$ and $\ln E$, with a linear relationship between them. Specifically, if we presume $\xi \sim N(0,1)$, and we approximate the marginal PDFs of $\ln A$ and $\ln E$ as Gaussians, then having a single degree of freedom in the statistics of A and E leads to the requirement

$$A = \exp(\mu_{\ln A} + \sigma_{\ln A}\xi) \tag{6}$$

$$E = \exp(\mu_{\ln E} + \sigma_{\ln E}\xi) \tag{7}$$

We will employ this dependence relationship for representing the uncertain A and E in the forward UQ problem below.

3. FORWARD UQ IN IGNITION

We use a mutiwavelet (MW) PC construction for the representation of random quantities over a block-decomposed stochastic space. We use this construction in an intrusive UQ context, employing Galerkin projection to arrive at reformulated governing equations for the PC modes. The method is outlined in detail in [30–32] and is briefly summarized below.

3.1. PC basics

We begin by defining a probability space $(\Omega, \mathfrak{S}, P)$, where Ω is a sample space, $\mathfrak{S}$ is a σ-algebra on Ω, and P is a probability measure on $(\Omega, \mathfrak{S})$. Further, define $\xi = \{\xi_i(\omega)\}_{i=1}^{\infty}$ as a set of independent standard normal RVs on Ω. Then we have that any RV $X : \Omega \to \mathbb{R}$ with finite variance can be represented as a doubly infinite spectral expansion in terms of the Wiener PC functionals [7, 13, 58]. This PCE may be written compactly as [13]

$$X(\omega) = \sum_{k=0}^{\infty} \alpha_k \Psi_k(\xi_1, \xi_2, \ldots) \tag{8}$$

where Ψ_k are the multi-dimensional Hermite polynomials, orthogonal with respect to the inner product

$$\langle u(\omega)v(\omega)\rangle = \int_{\Omega} u(\omega)v(\omega)\,\mathrm{d}P = \int u(\omega)v(\omega)\,p_{\xi}(\xi)\,\mathrm{d}\xi \tag{9}$$

where $p_{\xi}()$ is the PDF of ξ. The definition of ξ as Gaussian, and this orthogonality constraint, dictates that the Ψ_k are Hermite polynomials. Alternate pairs of RVs and corresponding orthogonal polynomials are given by the Askey scheme [26, 27]. This representation applies generally to random fields/processes $X(x,t,\omega)$ with finite variance, where the PC mode strengths become spatially/temporally dependent, $\alpha_k(x,t)$.

DOI: 10.1002/nme

In a computational context, the PCE is truncated in both order p and dimension n, resulting in a finite PCE$^{(n,p)}$

$$X(\omega) \approx \sum_{k=0}^{P} \alpha_k \Psi_k(\xi_1, \xi_2, \ldots, \xi_n) \tag{10}$$

with $P+1=(n+p)!/n!p!$ terms. Note that orthogonality of the Ψ_k allows the evaluation of the PC mode strengths employing Galerkin projection, namely

$$\alpha_k = \frac{\langle X\Psi_k \rangle}{\langle \Psi_k^2 \rangle} \tag{11}$$

This construction can be used to reformulate the governing equations of any given model with uncertain inputs/parameters, arriving at equations for the PC mode strengths of the solution. For illustration, consider an ordinary differential equation (ODE) system

$$\frac{\mathrm{d}u}{\mathrm{d}t} = g(u;\eta) \tag{12}$$

where $u \in \mathbb{R}^N$, $g() : \mathbb{R}^N \to \mathbb{R}^N$ is a smooth function, $u(t=0)=u^*$, and $\eta \in \mathbb{R}^L$ is a parameter vector. Then, given known PCEs$^{(n,p)}$ for $u^* = \sum_{k=0}^{P} u_k^* \Psi_k$ and $\eta = \sum_{k=0}^{P} \eta_k \Psi_k$, assuming unknown PCE$^{(n,p)}$ for $u = \sum_{k=0}^{P} u_k \Psi_k$, and applying Galerkin projection to the ODE system, we get

$$\frac{\mathrm{d}u_k}{\mathrm{d}t} = \frac{\langle g(u;\eta)\Psi_k \rangle}{\langle \Psi_k^2 \rangle}, \quad k=0,1,\ldots,P \tag{13}$$

where the right-hand side can be evaluated using spectral or pseudo-spectral constructions [59].

3.2. MW polynomial chaos

The MW extension of the above construction on a block-decomposed stochastic space results in a distinct PC representation on each block. Let $\Omega = [a_1, b_1] \times \cdots \times [a_n, b_n]$ be the space of $\xi = \{\xi_1, \ldots, \xi_n\}$ where ξ_d has the PDF $\pi_d(\xi_d)$ and CDF $p_d(\xi_d)$, and consider a partition of Ω into M non-overlapping subdomains $\Omega^m = [a_1^m, b_1^m] \times \cdots \times [a_n^m, b_n^m]$, $m=1,2,\ldots,M$. Given the independence of the ξ_i, the PDF of ξ on each block is defined as

$$\pi^m(\xi) = \prod_{d=1}^{n} \pi_d^m(\xi_d) \tag{14}$$

with

$$\pi_d^m(\xi_d) = \frac{\pi_d(\xi_d)}{p_d(b_d^m) - p_d(a_d^m)} \tag{15}$$

Then, with the CDF of ξ_d on block m defined as $p_d^m(\xi_d | \xi_d \in [a_b^m, b_b^m]) = \int_{a_d^m}^{\xi_d} \pi_d^m(\xi')d\xi'$, and defining the RV x_d^m uniformly distributed on $[0,1]$, it is seen that the RV $(p_d^m)^{-1}(x_d^m) \in [a_b^m, b_b^m]$ and has the PDF π_d^m. On any block Ω^m, we can locally expand any second-order RV u in terms

DOI: 10.1002/nme

of $x^m = \{x_1^m, x_2^m, \ldots, x_n^m\}$. Specifically, the MW$^{(n,p)}$ PCE for u, with first-level directional details, on Ω^m is given by [31]

$$u = \sum_{\lambda \in \gamma} u_\lambda^m \Phi_\lambda^m(x^m) + \sum_{d=1}^{n} \sum_{i=0}^{p} u_{d,i}^m \mathscr{D}_i(x_d^m) = \sum_{k=0}^{P} u_k \mathscr{W}_k^m(x^m) \tag{16}$$

where $\lambda = (\lambda_1, \ldots, \lambda_n)$ is a multi-index composed of non-negative integers

$$\gamma = \left\{ (\gamma_1, \ldots, \gamma_n) \,\middle|\, \sum_{d=1}^{n} \gamma_d \leqslant p \right\} \tag{17}$$

and there is a one-to-one correspondence between the $\mathscr{W}_k^m$ and the Φ_λ^m and $\mathscr{D}_i$ terms. Further

$$\Phi_\lambda^m(x^m) \equiv \prod_{d=1}^{n} \phi_{\lambda_d}(x_d^m) \tag{18}$$

where

$$\phi_i(x) = \frac{\mathfrak{L}_i(2x-1)}{L_i}, \quad i = 0, 1, \ldots, p \tag{19}$$

and $\mathfrak{L}_i()$ is the Legendre polynomial of degree i defined on $[-1, 1]$, namely

$$\mathfrak{L}_0(x) = 1, \quad \mathfrak{L}_1(x) = x \quad \text{and} \quad \mathfrak{L}_{i+1}(x) = \frac{2i+1}{i+1} x \mathfrak{L}_i(x) - \frac{i}{i+1} \mathfrak{L}_{i-1}(x) \tag{20}$$

and the $L_i = (2i+1)^{-1/2}$ are normalization factors ensuring orthonormality of the $\phi_i()$ over [0,1], such that

$$\langle \phi_i(x), \phi_j(x) \rangle \equiv \int_0^1 \phi_i(x) \phi_j(x) \, \mathrm{d}x = \delta_{ij} \tag{21}$$

Note also that

$$\langle \phi_i(x) \rangle \equiv \int_0^1 \phi_i(x) \, \mathrm{d}x = 0 \quad \text{for } i > 0 \tag{22}$$

The first-level directional wavelet details $\mathscr{D}_i$, which can be constructed following [31], are piecewise polynomial functions with degree less than or equal to p, satisfying, for $0 \leqslant i, j \leqslant p$

$$\langle \mathscr{D}_i(x), \mathscr{D}_j(x) \rangle \equiv \int_0^1 \mathscr{D}_i(x) \mathscr{D}_j(x) \, \mathrm{d}x = \delta_{ij} \tag{23}$$

$$\langle \mathscr{D}_j(x), x^i \rangle = 0 \tag{24}$$

where the last condition ensures $\langle \mathscr{D}_j(x), \phi_i(x) \rangle \equiv 0$, $\forall i, j$. Given the mutual orthonormality constraints on ϕ and $\mathscr{D}$, Equations (21), (23), (24), we have

$$u_\lambda^m = \langle u \Phi_\lambda^m \rangle_m \tag{25}$$

$$u_{d,i}^m = \langle u \mathscr{D}_i \rangle_{m,d} \tag{26}$$

DOI: 10.1002/nme

where $\langle\rangle_{m,d}$ is the above one-dimensional expectation applied on block m in direction d, whereas $\langle\rangle_m$ is the multi-dimensional expectation on block m, given by

$$\langle u\Phi^m_\lambda\rangle_m = \underbrace{\int_0^1 \dots \int_0^1}_{n} u\ \phi_{\lambda_1}\dots\phi_{\lambda_n}\,\mathrm{d}x^m_1\dots\mathrm{d}x^m_n \tag{27}$$

and where

$$\langle\Phi^m_\alpha\Phi^m_\beta\rangle_m = \prod_{d=1}^{n}\langle\phi^m_{\alpha_d}\phi^m_{\beta_d}\rangle_{m,d} \tag{28}$$

Note further that, on Ω^m, the local expectation of u is given by

$$\langle u\rangle_m = u^m_{0,\dots,0} \tag{29}$$

and its local variance is given by

$$\sigma^2_m(u) = \hat{\sigma}^2_m + \sum_{d=1}^{n}\tilde{\sigma}^2_{m,d} \tag{30}$$

where

$$\hat{\sigma}^2_m \equiv \sum_{\lambda\in\Delta}(u^m_\lambda)^2, \quad \tilde{\sigma}^2_{m,d} \equiv \sum_{i=0}^{p}(u^m_{d,i})^2 \tag{31}$$

with $\Delta = \gamma\backslash\{0,\dots,0\}$. The global mean is given by

$$\langle u\rangle = \sum_{m=1}^{M}\langle u\rangle_m \mathscr{V}_m \tag{32}$$

where

$$\mathscr{V}_m = \prod_{d=1}^{n}(p_d(b^m_d) - p_d(a^m_d)) \tag{33}$$

is the probability of ξ being in block Ω_m. The global variance is

$$\sigma^2(u) = \sum_{m=1}^{M}[\sigma^2_m(u) + (u^m_{0,\dots,0} - \langle u\rangle)^2]\mathscr{V}_m \tag{34}$$

Finally, note that the block refinement algorithm [31] relies on a measure of the magnitude of the uncertainty captured in the first-level details along a given direction relative to the total uncertainty in a given block. Using the local variances defined above, this measure, on block m and in direction d, is given by

$$\rho^d_m = \frac{\tilde{\sigma}_{m,d}}{\sigma_m} \tag{35}$$

The refinement algorithm splits a block in two equal halves along direction d if

$$\rho^d_m \geqslant \varepsilon/\mathscr{V}_m \tag{36}$$

where ε is a chosen threshold.

DOI: 10.1002/nme

With this basic outline of the multiwavelet PC construction, we proceed next to the specific implementation for the set of governing equations at hand.

3.3. PC reformulation of the governing equations

The PC reformulation of the full chemical source term was presented in [46]. Here, we present specifics relevant to the present context.

We write the set of equations governing the homogeneous ignition of a mixture of N-species in terms of the species mass fractions $\{Y_i\}_{i=1}^N$ and temperature T. Specifically

$$\frac{\mathrm{d}Y_i}{\mathrm{d}t} = \frac{w_i}{\rho} \quad \text{for } i = 1, 2, \ldots, N \tag{37}$$

$$\frac{\mathrm{d}T}{\mathrm{d}t} = \frac{w_T}{\rho c_p} \tag{38}$$

where the ideal gas state equation provides the density ρ as

$$\rho = \frac{P_0 \overline{W}}{R^0 T} \tag{39}$$

and where $R^0 = 8314.51\,\mathrm{J/kmol\,K}$ is the universal gas constant, $\overline{W} = 1/\sum_{i=1}^N Y_i W_i$ is the molar mass of the mixture, W_i is the molar mass of species i, and P_0 is the pressure. Assuming constant atmospheric-pressure ignition, we set $P_0 = 101\,325\,\mathrm{Pa}$. Further, $c_p = \sum_{i=1}^N Y_i c_{p_i}$ is the mixture specific heat, where $c_{p_i}(T)$ (J/kg K) is the specific heat of species i. The chemical source term for the energy equation is given by $w_T = -\sum_{i=1}^N h_i w_i$, where $h_i(T)$ (J/kg) is the enthalpy of species i. Finally, $w_i(Y_1, \ldots, Y_N, T)$ is the chemical source term for species i. The full formulation of w_i for a general chemical kinetic system is outlined elsewhere, e.g. [46]. For the present discussion, and as stated earlier, we presume a simple single-step global irreversible reaction mechanism for methane (Equation 1), such that the methane–air system includes only the $N = 5$ species $\{\mathrm{CH_4}, \mathrm{O_2}, \mathrm{CO_2}, \mathrm{H_2O}, \mathrm{N_2}\}$. With the reaction rate of progress as specified in Equation (3), and denoting the concentration of species i with $c_i = \rho Y_i / W_i$, we have

$$w_i = W_i \nu_i \mathscr{R} = W_i \nu_i c_1^x c_2^y k_f(T) \tag{40}$$

where ν_i is the stoichiometric coefficient of species i in the reaction, namely $\nu_i \in \{-1, -2, 1, 2, 0\}$. More specifically, with $x = y = 1$ and a zero temperature exponent, we have

$$w_i = W_i \nu_i c_1 c_2 A \mathrm{e}^{-E/R^0 T} \tag{41}$$

These equations are closed with the initial conditions $Y_i(t=0) = Y_i^0$ and $T(t=0) = T^0$.

From a numerical perspective, it is feasible in this system to enforce discrete mass conservation by employing Equation (37) only for the first $N-1$ species, while the mass fraction of the Nth species, N_2, is found from a mass conservation constraint, namely

$$Y_N = 1.0 - \sum_{i=1}^{N-1} Y_i \tag{42}$$

The reformulation of this system of equations using PC can be easily done using the pseudo-spectral Galerkin-projection approach employed in [46, 59]. The original (truncated) system of

DOI: 10.1002/nme

N ODEs for $(Y_1, \ldots, Y_{N-1}, T)$ is transformed into a system of $N(P+1)$ ODEs for the mode strengths of the PCEs of these state variables, where $(P+1)$ is the total number of terms in the MW PCE in Equation (16). With $Y_i = \sum_{k=0}^{P} Y_{i,k} \mathscr{W}_k^m$, $T = \sum_{k=0}^{P} T_k \mathscr{W}_k^m$, $A = \sum_{k=0}^{P} A_k \mathscr{W}_k^m$, and $E = \sum_{k=0}^{P} E_k \mathscr{W}_k^m$, the new equation system can be written compactly as

$$\frac{\mathrm{d}Y_{i,k}}{\mathrm{d}t} = \left\langle \left(\frac{w_i}{\rho} \right) \mathscr{W}_k^m \right\rangle_m \quad \text{for } i = 1, 2, \ldots, N-1,\ k = 0, 1, \ldots, P \tag{43}$$

$$\frac{\mathrm{d}T_k}{\mathrm{d}t} = \left\langle \left(\frac{w_T}{\rho c_p} \right) \mathscr{W}_k^m \right\rangle_m, \quad k = 0, 1, \ldots, P \tag{44}$$

The projection operations on the right-hand side can be evaluated given the algebraic forms of each term employing the pseudo-spectral operations in [46, 59]. These implementations of the pseudo-spectral construction were in the context of global PCEs. However, the formulation is equivalent with the utilization of the proper tensor product coefficients relevant to each case and has been similarly applied in the MW context in [32]. For illustration, and given its central role in the computation, we illustrate the pseudo-spectral evaluation of the PCE for the chemical source term, for $x = y = 1$ and zero temperature exponent. Given the PCEs for the uncertain quantities E, T, A, c_1, c_2, the evaluation of the PCE modes of w_i in block m, per Equation (41), is done using the following steps:

$$s = \sum_{k=0}^{P} s_k \mathscr{W}_k^m = -\frac{E}{R^0 T} \quad \text{where } s_k = -\frac{1}{R^0} \left\langle \frac{E}{T} \mathscr{W}_k^m \right\rangle_m \quad \forall k \tag{45}$$

$$r = \sum_{k=0}^{P} r_k \mathscr{W}_k^m = e^s \quad \text{where } r_k = \langle e^s \mathscr{W}_k^m \rangle_m \quad \forall k \tag{46}$$

$$k_f = \sum_{k=0}^{P} k_{f,k} \mathscr{W}_k^m = Ar \quad \text{where } k_{f,k} = \langle Ar \mathscr{W}_k^m \rangle_m \quad \forall k \tag{47}$$

$$g = \sum_{k=0}^{P} g_k \mathscr{W}_k^m = c_2 k_f \quad \text{where } g_k = \langle c_2 k_f \mathscr{W}_k^m \rangle_m \quad \forall k \tag{48}$$

$$w_i = \sum_{k=0}^{P} w_{i,k} \mathscr{W}_k^m = W_i \nu_i c_1 g \quad \text{where } w_{i,k} = W_i \nu_i \langle c_1 g \mathscr{W}_k^m \rangle_m \quad \forall k \tag{49}$$

Given the PCEs of any two uncertain quantities u and v, this sequence requires algorithms for evaluating the PCE modes of u/v, e^u, and uv. These algorithms are outlined in [59].

Further, we note that the mass conservation constraint is also transformed to

$$Y_{N,0} = 1.0 - \sum_{i=1}^{N-1} Y_{i,0} \tag{50}$$

$$Y_{N,k} = -\sum_{i=1}^{N-1} Y_{i,k}, \quad k = 1, \ldots, P \tag{51}$$

DOI: 10.1002/nme

as there is no uncertainty in the sum of the uncertain Y_i; it is a deterministic unity. All of this, of course, is done on each block Ω_m independently.

4. APPLICATION TO METHANE–AIR IGNITION

We set up the homogeneous ignition problem for the methane–air mixture with a deterministic initial condition corresponding to a stoichiometric mixture at 1050 K. Thus, the initial state vector is $(0.055, 0.22, 0, 0, 0.725, 1050)$. Further, we set up the two uncertain parameters (A, E) dependent on a single stochastic degree of freedom ξ, as in Equation (7). With $n=1$, the first summation in Equation (16) has $(p+1)$ terms, such that the total number of terms in the PCE is $P+1=2(p+1)$. We use fourth-order MW PC, i.e. $p=4$, and a block-refinement threshold $\varepsilon=0.005$. As will be seen, statistics of the uncertain ignition process computed with these values of p and ε agree well with sampled Monte Carlo (MC) statistics of the deterministic system. Finally, with zero initial uncertainty, the initial condition requires only one block, i.e. $M=1$.

We integrate the reformulated PC equations using DVODE [60] employing implicit time integration with adaptive time stepping and error control. An external time-stepping loop advances the solution in time at a coarse time step Δt_c, and DVODE is employed to advance the solution internally within each Δt_c. The time evolution of the mean temperature value is used to further adapt the choice of Δt_c to maintain sufficient time resolution in the reported solution and to ensure a given upper limit of internal DVODE time steps. As the time integration proceeds, the block refinement check is done at the end of each Δt_c. Following the block refinement algorithm in [32], if a given block is found to require refinement per the criterion (36), it is split into two blocks and the coarse time step is repeated for each of the daughter blocks, while other blocks are unaffected. However, this check is not done at every internal DVODE time step. As a result, and because of the fast time scales involved in the present system, the DVODE internal time integration of the MW PC system within a given block can lead to values that result in failure of the pseudo-spectral PC algebra [59] for the chemical source term. When this occurs, it is easily remedied, by again flagging block refinement and repeating the coarse time step for the two daughter blocks. Thus, with this overall block-refinement strategy, starting at t^n, the integrator proceeds looping over available blocks until all blocks, including old and new ones, reach $t^{n+1}=t^n+\Delta t_c$.

4.1. Moments

Using the mean and standard deviations of $\ln A$ and $\ln E$ identified from the Bayesian parameter estimation, we integrate the above system of equations over a 1 s time span. The time evolution of the mean values of the species mass fractions and temperature is shown in Figure 5, whereas the corresponding time evolution of the standard deviations is shown in Figure 6. The means illustrate the fast ignition transient in all elements of the state vector. The standard deviations exhibit initial growth from zero, given the deterministic initial condition. A long initial slow uncertainty growth phase corresponds to the induction time prior to ignition, where the means exhibit similar slow rates of change. A rapid growth of the standard deviations is observed as the ignition process enters the fast transient mode at around 0.465 s. The standard deviation in the temperature reaches a peak of 400 K before exhibiting fast decay back to zero. Similar behavior is evident in the species mass fractions. All standard deviation values decay to zero as the system approaches its equilibrium state. Since uncertainty was included only in the kinetic rate constants, and the thermodynamic

DOI: 10.1002/nme

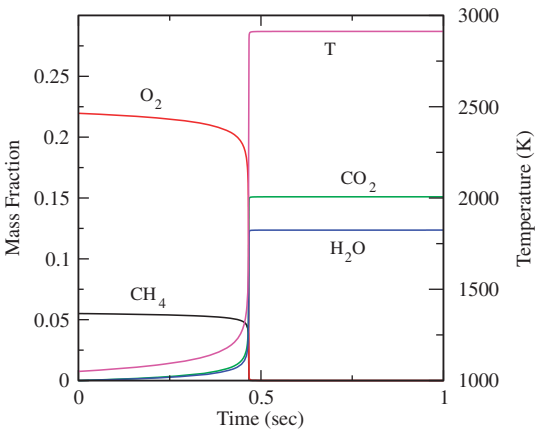

Figure 5. Time evolution of mean values of the species mass fractions and temperature.

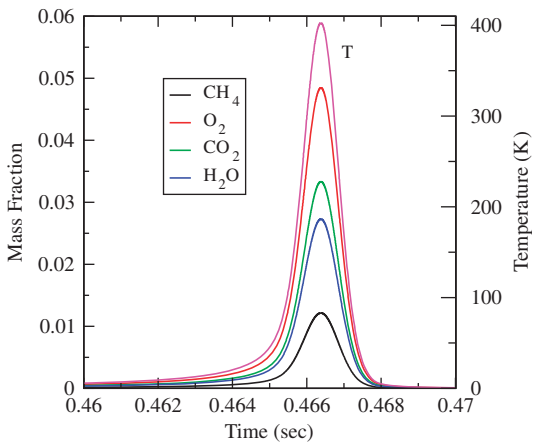

Figure 6. Time evolution of the standard deviation values of the species mass fractions and temperature.

quantities had no inherent uncertainty, it follows that there is no uncertainty in the equilibrium state, only in the path toward equilibrium. The results are consistent with this expectation.

4.2. Probability density functions

In order to better understand the structure of the uncertain solution, we examine the time evolution of the PDFs of the species mass fractions and temperature. PDFs are computed by random sampling of the MW PCE of each component of the state vector, at any given time instant, and binning the resulting samples. The PDFs of temperature are shown for a subset of the initial time period in Figure 7. We illustrate the PDFs evaluated from the PC solution as well as those available from MC sampling of the deterministic ignition problem, with the prescribed uncertain parameters and given initial values. The results in the figure illustrate agreement between the two solutions in the

DOI: 10.1002/nme

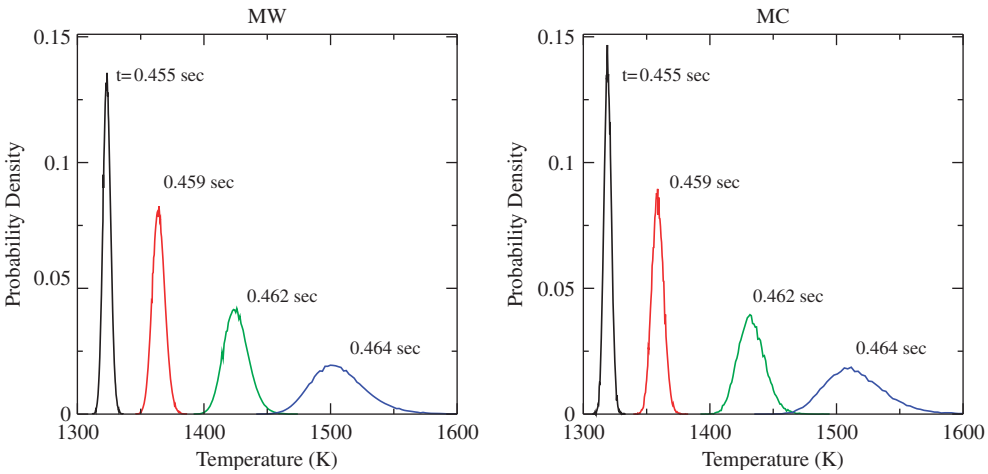

Figure 7. Time evolution of the temperature PDF during the pre-ignition phase. Results are shown from multiwavelet (MW) and Monte Carlo (MC) computations, for $\mu_{\ln A} = 34.10316$, $\mu_{\ln E} = 10.817866$, $\sigma_{\ln A} = 2.28 \times 10^{-3}$, and $\sigma_{\ln E} = 6.86 \times 10^{-5}$.

structure and time evolution of the temperature PDFs over this time period immediately preceding the fast ignition transient. The temperature PDF is observed to both shift toward higher temperature values and exhibit larger uncertainty as time progresses, reflecting the above illustrated growth in the mean and standard deviation of temperature during this time period. At the same time, the figure illustrates the tendency of the PDF to become more skewed, exhibiting a longer tail toward high temperature, as time advances. Examination of the PDFs of other components of the state vector reveals similar findings.

The time evolution of the temperature PDFs during the fast transient phase is shown in Figure 8. The results illustrate a bimodality in the solution PDFs involving large probability mass centered around the pre- and post-ignition states of the system. The slightly skewed PDF from the earlier phase of slow growth shown in Figure 7, corresponding to the unburnt state of the system, develops significantly more skewness and a long tail toward the burnt state. The PDF 'leaks' probability mass to the burnt state, where a new PDF peak is observed to grow in time, while the initial unburnt PDF peak diminishes in concert. This transfer leads eventually to a single peak centered on the burnt state. This bimodal behavior is also observed in the MC results, also included in the figure. It is primarily a consequence of the fast, highly activated, kinetics, where extreme sensitivity to temperature, strong non-linearity, and fast ignition, lead to near-zero probability of being anywhere in the intermediate region between the unburnt and burnt states.

4.3. Dependence

Note that capturing the true dependence relationship among the parameters can be crucially important to the accurate computation of the uncertainty in model predictions. Having assumed, based on the Bayesian analysis of the data, a perfect correlation, and an associated linear dependence relationship, between the two parameters $\ln A$ and $\ln E$, and fixing the mean parameter estimates $(\mu_{\ln A}, \mu_{\ln E})$ at those found from the Bayesian analysis, this linear dependence is completely

DOI: 10.1002/nme

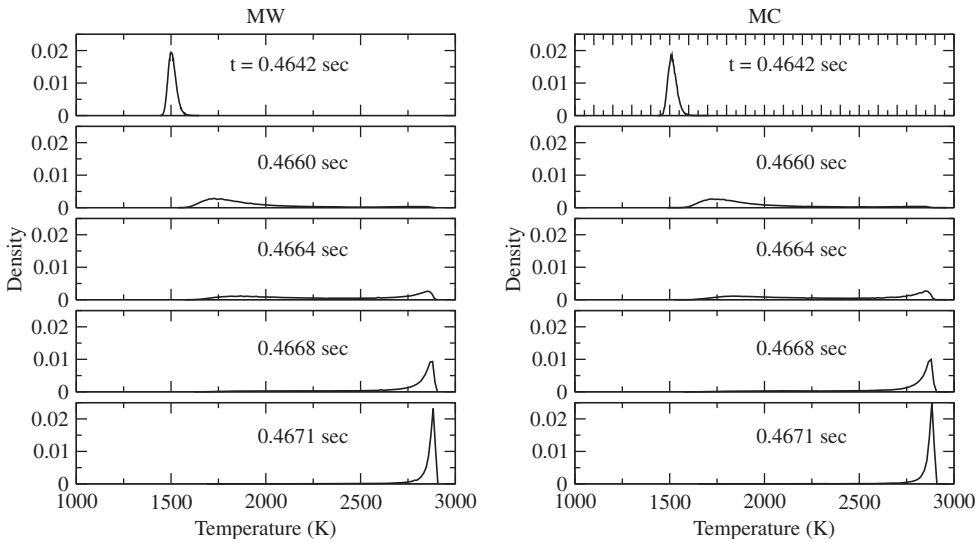

Figure 8. Time evolution of the temperature PDF during the ignition transient. Results are shown from multiwavelet (MW) and Monte Carlo (MC) computations, for $\mu_{\ln A} = 34.10316$, $\mu_{\ln E} = 10.817866$, $\sigma_{\ln A} = 2.28 \times 10^{-3}$, and $\sigma_{\ln E} = 6.86 \times 10^{-5}$.

prescribed by the ratio of the standard deviations of the two parameters. Specifically, consider the ratio defined as

$$\chi \equiv \frac{\sigma_{\ln E}}{\sigma_{\ln A}} \tag{52}$$

Given the imposed parametric uncertainty

$$\ln A = \mu_{\ln A} + \sigma_{\ln A}\xi \tag{53}$$

$$\ln E = \mu_{\ln E} + \sigma_{\ln E}\xi \tag{54}$$

we have the following relationship between A and E:

$$\frac{\ln E - \mu_{\ln E}}{\ln A - \mu_{\ln A}} = \chi \tag{55}$$

Given the structure of the Arrhenius rate model, the value of χ has a significant effect on the sensitivity of the time trajectory of the system on ξ. In particular, using the $(\mu_{\ln A}, \mu_{\ln E}, \sigma_{\ln A})$ identified from the Bayesian parameter estimation, consider varying $\sigma_{\ln E}$ employing

$$\sigma_{\ln E} = \chi \sigma_{\ln A} \tag{56}$$

over a range of χ. This will retain a specific marginal PDF for $\ln A$, while varying the marginal PDF of $\ln E$, and the slope of the linear relationship between $\ln A$ and $\ln E$, always retaining a perfect correlation between them. One can alternatively fix $\sigma_{\ln E}$ and let $\sigma_{\ln A}$ vary with χ. However, a single parametric study, with fixed $\sigma_{\ln A}$, suffices to highlight the role of χ.

DOI: 10.1002/nme

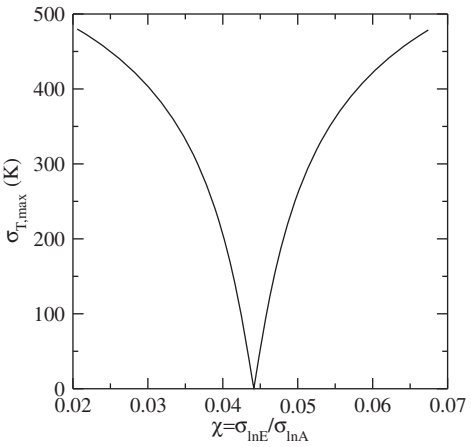

Figure 9. Dependence of $\sigma_{T,\max}$ on $\chi = \sigma_{\ln E}/\sigma_{\ln A}$, with $\mu_{\ln A} = 34.10316$, $\mu_{\ln E} = 10.817866$, $\sigma_{\ln A} = 2.28 \times 10^{-3}$, and $T_0 = 1050\,\mathrm{K}$.

For every choice of χ, we solve the forward UQ ignition problem as done above, and examine the evolution of the uncertain solution in time. Consider specifically the maximum standard deviation of temperature, $\sigma_{T,\max}$, during the ignition process, which is plotted versus χ in Figure 9. Remarkably, starting at around $\chi = 0.02$, where $\sigma_{T,\max} \approx 500\,\mathrm{K}$, increasing χ, and therefore *increasing* $\sigma_{\ln E}$ leads to a *reduced* $\sigma_{T,\max}$. Moreover, this reduction is maintained up till $\chi \approx 0.044$, for which $\sigma_{T,\max} \approx 0$. Evidently, for this particular χ value there is no discernible uncertainty in the resulting temperature field over time. Increasing χ beyond this value leads to an increasing $\sigma_{T,\max}$ in a roughly symmetric fashion around $\chi = 0.044$.

The impact of the dependence relationship between the parameters can be further understood by examining the temporal evolution of the PDFs of the temperature field for different χ values. This information is presented in Figure 10. Each frame in the figure corresponds to a given χ over the range of values in Figure 9, as indicated. Starting with low χ, in the vicinity of 0.02, we find the same bimodal behavior observed above. Starting at early time with a unimodal temperature PDF centered at low temperature, the solution progresses through a bimodal phase with probability density accumulating at high temperature, and diminishing at low temperature, with little probability of being at intermediate temperature values. As χ is increased, the relative amplitude of probability density at intermediate values is found to increase. By $\chi \approx 0.042$, the bimodal phase is absent entirely, with the temperature PDF going through a low temperature phase skewed toward high temperature, to a symmetric broad shape in the intermediate temperature region ($\sim 2300\,\mathrm{K}$), to a high temperature phase skewed toward low temperature at late time. Increasing χ further toward 0.044 leads to a reduction in skewness and width of the evolving temperature PDF, with much reduced σ_T throughout the time evolution. The former phases of behavior are observed, in reverse order, as χ is increased further beyond 0.044, retrieving the bimodal time evolution observed at low χ values. Thus, the uncertain solution structure is *strongly* dependent on the specific dependence between A and E.

Further inquiry into the dependence of the ignition solution on (A, E) clarifies the reasons behind the above observed behavior. Consider the deterministic ignition process for a given pair

DOI: 10.1002/nme

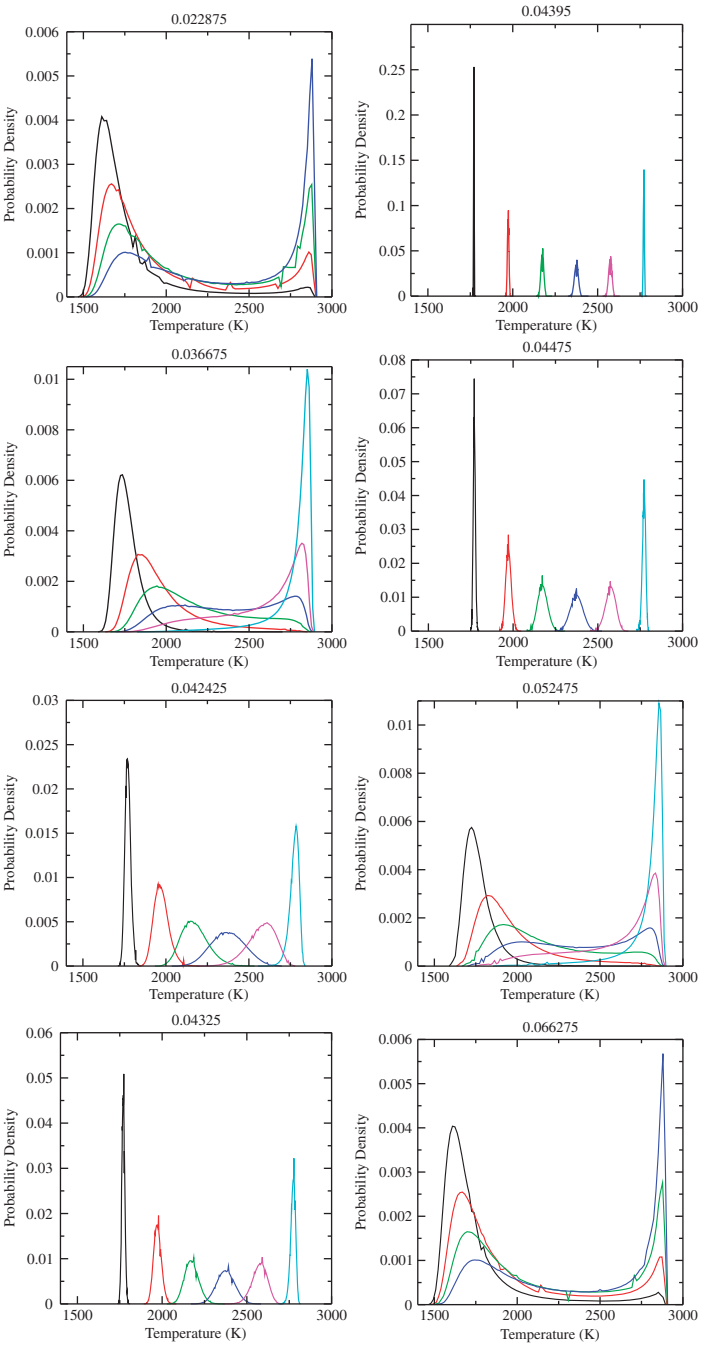

Figure 10. Time evolution of the temperature PDFs at different ratios of $\chi = \sigma_{\ln E}/\sigma_{\ln A}$. The χ-values are indicated above each frame.

DOI: 10.1002/nme

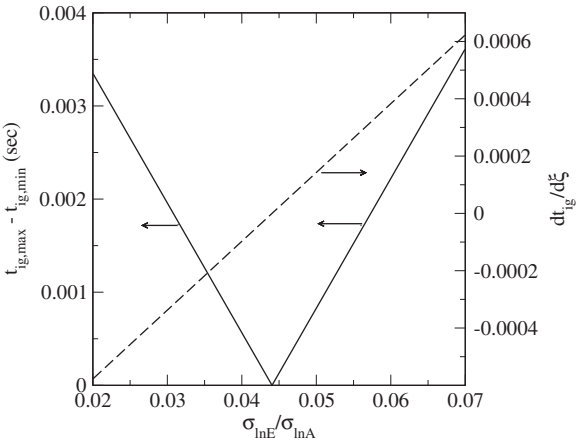

Figure 11. Dependence of the ignition time t_{ig} on sampled $A(\xi)$, $E(\xi)$ for $\xi \in [-3, 3]$. Plot of $dt_{ig}/d\xi$ (dashed line) and maximum variation in t_{ig} for $\xi \in [-3, 3]$ (solid line), versus $\chi = \sigma_{\ln E}/\sigma_{\ln A}$.

(A, E), and let us define the ignition time, t_{ig}, as the time at which the temperature reaches a set value, say 1500 K. Further, consider parametric variation of (A, E) with $\xi \in [-3, 3]$ employing Equations (53), (54). In fact, in the vicinity of the given $(\mu_{\ln A}, \mu_{\ln E})$, and for this $\pm 3\sigma$ variation in ξ, numerical computations of deterministic ignition in this system show that t_{ig} varies inversely with A, but directly with E, such that its net dependence on ξ is non-trivial. Depending on the value of χ, one or the other trend may win in the dependence of t_{ig} on ξ. In fact, for $\sigma_{\ln A} = 2.28 \times 10^{-3}$, and varying χ over the range [0.02,0.07] explored above, we find that t_{ig} exhibits linear dependence on ξ with a slope $dt_{ig}/d\xi$ which varies linearly with χ, being negative/positive at low/high χ, and zero for $\chi = \chi^* \approx 0.044$, as shown in Figure 11. Thus, given $\sigma_{\ln A}$, for low $\chi < \chi^*$, $dt_{ig}/d\xi < 0$ such that increasing ξ leads to decreased t_{ig}. In this case, given the low $\sigma_{\ln E}$ values, the overall dependence of t_{ig} on ξ is dominated by the inverse dependence on A. On the other hand, the opposite is observed at high χ, and therefore high $\sigma_{\ln E}$ values, where $dt_{ig}/d\xi$ is dominated by the direct dependence of t_{ig} on E. The two trends cancel at $\chi = \chi^*$ for the chosen mean conditions, with $dt_{ig}/d\xi = 0$. The figure also shows the dependence of the observed change in t_{ig} over the range of ξ, namely $\Delta_\xi t_{ig} = t_{ig,max} - t_{ig,min}$, on χ. We see that, at $\chi^* \approx 0.044$, $\Delta_\xi t_{ig} = 0$, such that there is no effect of ξ on the ignition time. On the other hand, for $\chi \sim 0.02$ or 0.07, t_{ig} varies by about 3 ms over the range of ξ.

Note that the variation in the ignition time with ξ is clearly determined by the dependence of the Arrhenius rate expression on $A(\xi)$ and $E(\xi)$. With zero temperature exponent, $k_f = Ae^{-E/R^0T}$, such that requiring $\partial k/\partial \xi|_T = 0$, along with the above dependence of $\ln A$ and $\ln E$ on ξ, leads to $\chi = \chi_0 = R^0T/E$. While T varies throughout the ignition process, this linear dependence of χ_0 on T, and the inverse dependence on E, is consistent with the observed variation of χ^* with the initial temperature, and $e^{\mu_{\ln E}}$ (not shown). Furthermore, no empirical dependence of χ^* on A is observed, again consistent with this analytical expression for χ_0.

4.4. Non-linearity and block refinement

It is instructive to examine the behavior of the solution for a case with a higher pre-exponential Arrhenius rate constant, leading to faster time scales in the ignition process. Specifically, consider

DOI: 10.1002/nme

the ignition of the same above stoichiometric methane–air mixture, but with an initial temperature of 800 K, employing $y=2$ in Equation 3 and with $\mu_{\ln A}=\ln(9\times10^{23})$, while $\sigma_{\ln A}$ and $\mu_{\ln E}$ are held at the above values, and $\sigma_{\ln E}=\chi\sigma_{\ln A}$ for any chosen χ. While this high rate constant is artificial, it is instructive to examine faster reaction rates, as elementary reaction rates in detailed chemical mechanisms are typically much faster than the time scale of the present global mechanism. With these changes, the time scale of the ignition process at the nominal conditions is accelerated from an original time scale of $[T/(\mathrm{d}T/\mathrm{d}t)]_{\max}\sim2.4\,\mathrm{ms}$, to $\sim0.14\,\mathrm{ms}$.

Figure 12 shows the dependence of the maximum standard deviation of temperature on χ. This system has a $\chi^*\approx0.0331$, which can be seen both in this figure and in the analysis of t_{ig} dependence

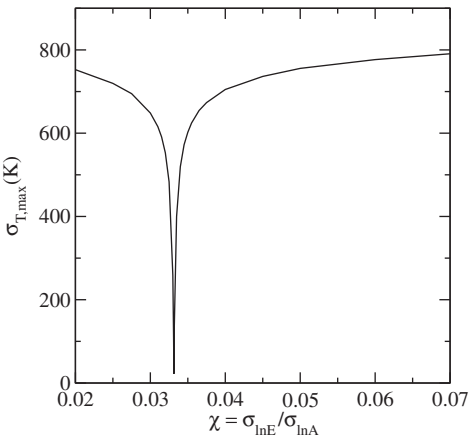

Figure 12. Variation of $\sigma_{T,\max}$ with χ for the case with stronger source term and increased non-linearity.

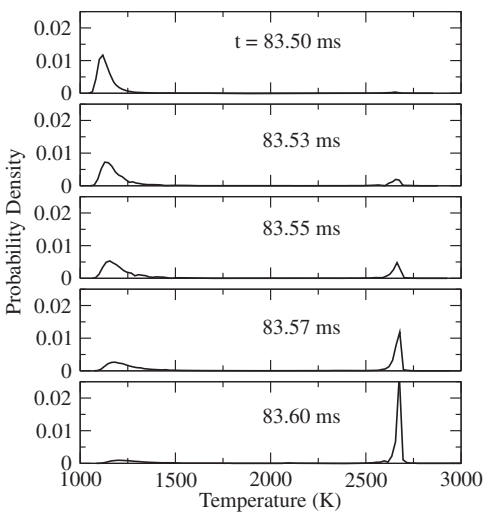

Figure 13. Time evolution of the temperature PDF over the short ignition transient, for $\chi=0.04$ in Figure 12.

DOI: 10.1002/nme

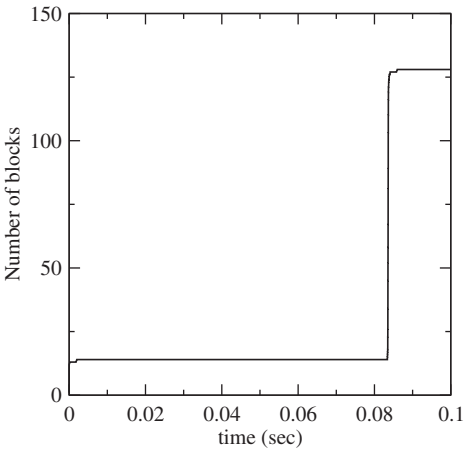

Figure 14. Time evolution of the number of blocks during the full ignition process, for $\chi = 0.04$ in Figure 12.

on $A(\xi)$ and $E(\xi)$ as done above. This change in χ^* reflects the change in initial temperature and the linear analytical dependence of χ_0 on T. The figure also highlights a generally higher maximum standard deviation of temperature and a steeper valley around χ^*, as compared with the above case.

Consider next specifically the case with $\chi = 0.04$. The time evolution of the PDFs of the temperature field is shown in Figure 13. While this plot is qualitatively similar to that in Figure 7, quantitative differences are evident in the larger separation between the two PDF peaks, with fast ignition leading to the appearance of the high temperature peak, while the low peak is still peaked at low temperature. By contrast, the results in Figure 7, with slower ignition time scales, exhibit a much smoother transition between the two peaks, where the low temperature peak is largely broadened and shifted to higher temperatures before the high temperature peak begins to become significant. The consequence of increased non-linearity, and faster time scales, in the uncertain ignition process is to lead to lower probability of being anywhere between the low temperature and high temperature peaks.

Another benefit of this case is that it illustrates succinctly the performance of the MW PC block-refinement strategy. Figure 14 shows the time evolution of the number of blocks during the ignition process. After an initial refinement phase, ending with 14 blocks after $t = 0.01$ s, no additional blocks are introduced during the long induction time prior to ignition. This is followed by a short period where many more blocks are introduced. This is precisely during the ignition process outlined in Figure 13 at the end of which the solution employs 128 blocks. The following phase, with reduced uncertainty as the solution tends to equilibrium has no added blocks. Clearly, the block refinement is proceeding in order to capture the changes in the uncertain state of the system during the ignition phase. In fact, the locations of the blocks successively refined during the fast uncertain ignition transient, illustrated in Figure 15, are quite instructive. The figure shows the time evolution of the block subdivision of the [0,1] space of the CDF of ξ, $p(\xi)$, during the ignition transient, with individual frames at the same instances as those in Figure 13. Clearly, block refinement proceeds from low ξ values at early time toward higher ξ values at later times during

DOI: 10.1002/nme

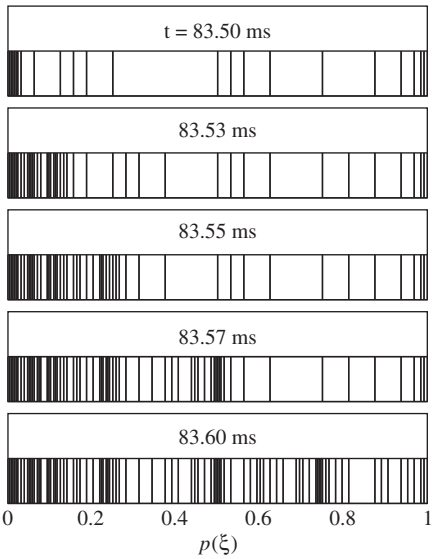

Figure 15. Time evolution of the block decomposition of the [0,1] space, for $\chi = 0.04$ in Figure 12.

the fast transient. This is quite consistent with the observation that, given the present specified linear dependence between the parameters, and with $\chi = 0.04$, we find $\mathrm{d}t_{\mathrm{ig}}/\mathrm{d}\xi > 0$. Thus, the block refinement proceeds initially at low ξ values because these reflect realizations of (A, E) which ignite early. Refinement progresses forward in ξ-space, reflecting the forward time-progress of t_{ig}, corresponding to the associated $(A(\xi), E(\xi))$ realizations. By the end of the ignition transient, refinement reaches large ξ values, by which time the [0,1] space is roughly uniformly refined, as seen in Figure 15.

Note that the results in Figure 15 outline a clear need for block *coarsening*, which is not included in the present algorithm, as there is no need to retain high block resolution in regions where the solution is already ignited. A block coarsening algorithm would improve the overall efficiency of the construction, with the corresponding refinement pattern in Figure 15 resembling more a translating narrow region of high refinement rather than the presently observed advancing front of a broad highly refined region. The computational performance of the algorithm depends directly on the number of blocks, such that a more parsimonious refinement/coarsening strategy would improve computational efficiency.

Another key aspect affecting performance is the time integration strategy. While the present construction can demonstrably provide accurate time integration of the MW PC system, computational cost increases, due to the need for smaller time steps, as one moves away from χ^* and the maximum standard deviation increases. This is true for both $\mu_{\ln A}$ cases studied above, but is more severe in this last case with higher $\mu_{\ln A}$ and faster time scales. Moreover, at sufficiently high $|\chi - \chi^*|$, e.g. beyond $\chi \approx 0.07$ in Figure 9, or for sufficiently high standard deviation in the solution, the time integration strategy can fail, with the implicit time integrator failing to satisfy requisite accuracy thresholds at any internal time step within machine precision (i.e. where $t + \Delta t \neq t$). These issues, of computational efficiency and robustness of the time integrator, require focused further study, and are outside the scope of the present work.

DOI: 10.1002/nme

5. CONCLUSIONS

We have presented a detailed study of probabilistic uncertainty quantification (UQ) in a model methane–air chemical system using a multiwavelet polynomial chaos (PC) construction. We employed a Bayesian methodology, using an adaptive MCMC procedure, to infer the joint PDF of model parameters of interest, starting from simulated noisy data. This PDF was used to construct a probabilistic representation of the uncertain parameters. We used a MW PC UQ methodology on a block-decomposed stochastic space to propagate this uncertainty through the chemical system model. The governing species and energy equations were reformulated using Galerkin projection into requisite equations for the MW PC mode strengths employing pseudo-spectral operations. We used an implicit time integration strategy to compute the evolution of the MW PC modes in time during an ignition event, and studied the evolution of the solution PDFs under a range of conditions.

Bayesian inference results provided marginal joint and individual PDFs of the parameters, thereby providing the requisite probabilistic characterization of parametric uncertainty. The marginal joint posterior PDF illustrated strong correlation between the two parameters. This posterior shape was found to present significant challenges for the conventional MCMC procedure, necessitating the use of adaptive MCMC. The two-dimensional marginal joint parametric PDF structure informed the formulation of a probabilistic model of the uncertainty in the two parameters, employing perfect correlation, with an explicit linear dependence relationship.

Forward UQ results provided the first demonstration of 'intrusive' PC UQ computations of non-isothermal ignition in a chemical system. Computed statistics were found to be in good agreement with MC sampling of the deterministic system with the given parametric uncertainties. Results highlight the fast growth of the means and standard deviations of the solution components during the fast ignition phase. The PDFs of the uncertain solution were found to evolve through a bimodal phase during the ignition event, with high probability of being at either low or high temperature but much less probability of being anywhere in between.

This bimodal character, and the extent of growth of uncertainty during the ignition event, were found to depend on the prescribed dependence relationship between the uncertain parameters. We outlined how the ignition time dependence on the two parameters leads to this observation. These results clearly indicate the importance of capturing the correct dependence among uncertain parameters, i.e. that dependence dictated by the model structure and available experimental/observational data, for accurate prediction of uncertainty in model outputs. We submit that these findings, while employing an idealized perfect correlation between the parameters, are generally relevant as regards the role of dependence relationships among parameters in UQ. While computations with an imperfect correlation would likely not exhibit a reduction of maximum uncertainty down to zero, as seen above for $\chi = \chi^*$, we expect that they would exhibit variation of $\sigma_{\max}$ with χ with some similarity to the above observations, depending on the degree of correlation.

Results have also illustrated the performance of the construction in the context of increased non-linearity and faster time scales in the chemical system. These computations generally exhibited higher $\sigma_{\max}$ and more distinct solution PDF bimodality during the ignition process. They also illustrated the performance of the block refinement strategy, capturing regions of high activity in probabilistic space at different time instances.

This study motivates further work in this area, toward more efficient and robust constructions enabling effective PC-based UQ in more detailed chemical and reacting flow systems of practical relevance, with higher dimensionality and increased model complexity.

DOI: 10.1002/nme

ACKNOWLEDGEMENTS

This work was supported by the US Department of Energy (DOE), Office of Basic Energy Sciences, Division of Chemical Sciences, Geosciences, and Biosciences. Sandia National Laboratories is a multi-program laboratory operated by Sandia Corporation, a Lockheed Martin Company, for the US DOE under contract DE-AC04-94-AL85000.

REFERENCES

1. Turányi T. Sensitivity analysis of complex kinetic systems—tools and applications. *Journal of Mathematical Chemistry* 1990; **5**:203–248.
2. Campolongo F, Saltelli A, Sørensen T, Tarantola S. Hitchhiker's guide to sensitivity analysis. In *Hitchhiker's Guide to Sensitivity Analysis*, Saltelli A, Chan K̃, Scott EM (eds). Wiley: Chichester, 2000.
3. Hills RG, Trucano TG. Statistical validation of engineering and scientific models: background. *Technical Report SAND99-1256*, Sandia National Labs., Albuquerque, NM, U.S.A., 1999.
4. Atherton RW, Shainker RB, Ducot ER. On the statistical sensitivity analysfis of models for chemical kinetics. *AIChE Journal* 1975; **21**(3):441–448.
5. Brown MJ, Smith DB, Taylor SC. Influence of uncertainties in rate constants on computed burning velocities. *Combustion and Flame* 1999; **117**(3):652–656.
6. Turányi T, Zalotai L, Dóbé S, Bérces T. Effect of uncertainty of kinetic and thermodynamic data on methane flame simulation results. *Physical Chemistry Chemical Physics* 2002; **4**:2568–2578.
7. Wiener N. The homogeneous chaos. *American Journal of Mathematics* 1938; **60**:897–936.
8. Cameron RH, Martin WT. The orthogonal development of nonlinear functionals in series of Fourier–Hermite functionals. *Annals of Mathematics* 1947; **48**:385–392.
9. Chorin AJ. Hermite expansions in Monte Carlo computation. *Journal of Computational Physics* 1971; **8**:472–482.
10. Maltz FH, Hitzl DL. Variance reduction in Monte Carlo computations using multi-dimensional Hermite polynomials. *Journal of Computational Physics* 1979; **32**:345–376.
11. Meecham WC, Jeng DT. Use of the Wiener–Hermite expansion for nearly normal turbulence. *Journal of Fluid Mechanics* 1968; **32**:225–249.
12. Chorin AJ. Gaussian fields and random flow. *Journal of Fluid Mechanics* 1974; **63**:21–32.
13. Ghanem RG, Spanos PD. *Stochastic Finite Elements*: *A Spectral Approach*. Springer: New York, 1991.
14. Ghanem R. Probabilistic characterization of transport in heterogeneous media. *Computer Methods in Applied Mechanics and Engineering* 1998; **158**:199–220.
15. Ghanem R. Ingredients for a general purpose stochastic finite element formulation. *Computer Methods in Applied Mechanics and Engineering* 1999; **168**:19–34.
16. Ghanem R. Stochastic finite elements for heterogeneous media with multiple random non-Gaussian properties. *Journal of Engineering Mechanics* (ASCE) 1999; **125**:26–40.
17. Ghanem RG, Red-Horse JR, Sarkar A. Modal properties of a space–frame with localized system uncertainties. In *8th ASCE Specialty Conference of Probabilistic Mechanics and Structural Reliability*, Kareem A, Haldar A, Spencer Jr BF, Johnson EA (eds). ASCE: New York, 2000. Number PMC200-269.
18. Sakamoto S, Ghanem R. Polynomial chaos decomposition for the simulation of non-Gaussian nonstationary stochastic processes. *Journal of Engineering Mechanics* 2002; **128**(2):190–201.
19. Le Maître OP, Knio OM, Najm HN, Ghanem RG. A stochastic projection method for fluid flow I. Basic formulation. *Journal of Computational Physics* 2001; **173**:481–511.
20. Le Maître OP, Reagan MT, Najm HN, Ghanem RG, Knio OM. A stochastic projection method for fluid flow II. Random process. *Journal of Computational Physics* 2002; **181**:9–44.
21. Debusschere B, Najm H, Matta A, Shu T, Knio O, Ghanem R, Le Maître O. Uncertainty quantification in a reacting electrochemical microchannel flow model. *Proceedings of the 5th International Conference on Modeling and Simulation of Microsystems*, San Juan, PR, 2002; 384–387.
22. Debusschere BJ, Najm HN, Matta A, Knio OM, Ghanem RG, Le Maître OP. Protein labeling reactions in electrochemical microchannel flow: numerical simulation and uncertainty propagation. *Physics of Fluids* 2003; **15**(8):2238–2250.
23. Ghiocel DM, Ghanem RG. Stochastic finite-element analysis of seismic soil–structure interaction. *Journal of Engineering Mechanics* 2002; **128**(1):66–77.

DOI: 10.1002/nme

24. Reagan MT, Najm HN, Ghanem RG, Knio OM. Uncertainty quantification in reacting flow simulations through non-intrusive spectral projection. *Combustion and Flame* 2003; **132**:545–555.
25. Xiu D, Lucor D, Su C-H, Karniadakis GE. Stochastic modeling of flow–structure interactions using generalized polynomial chaos. *Journal of Fluids Engineering* (ASME) 2002; **124**:51–59.
26. Askey R, Wilson J. Some basic hypergeometric polynomials that generalize Jacobi polynomials. *Memoirs of the American Mathematical Society* 1985; **319**:1–55.
27. Schoutens W. *Stochastic Processes and Orthogonal Polynomials*. Springer: Berlin, 2000.
28. Xiu D, Karniadakis GE. Modeling uncertainty in steady state diffusion problems via generalized polynomial chaos. *Computer Methods in Applied Mechanics and Engineering* 2002; **191**:4927–4948.
29. Xiu D, Karniadakis GE. The Wiener–Askey polynomial chaos for stochastic differential equations. *SIAM Journal on Scientific Computing* 2002; **24**(2):619–644.
30. Le Maître OP, Ghanem RG, Knio OM, Najm HN. Uncertainty propagation using Wiener–Haar expansions. *Journal of Computational Physics* 2004; **197**(1):28–57.
31. Le Maître OP, Najm HN, Ghanem RG, Knio OM. Multi-resolution analysis of Wiener-type uncertainty propagation schemes. *Journal of Computational Physics* 2004; **197**:502–531.
32. Le Maître OP, Najm HN, Pébay PP, Ghanem RG, Knio OM. Multi-resolution-analysis scheme for uncertainty quantification in chemical systems. *SIAM Journal on Scientific Computing* 2007; **29**(2):864–889.
33. Wan X, Karniadakis GE. An adaptive multi-element generalized polynomial chaos method for stochastic differential equations. *Journal of Computational Physics* 2005; **209**:617–642.
34. Mathelin L, Hussaini MY. A stochastic collocation algorithm for uncertainty analysis. *Technical Report*, *NASA/CR-2003-212153*, 2003.
35. Mathelin L, Hussaini MY, Zang TA. Stochastic approaches to uncertainty quantification in CFD simulations. *Numerical Algorithms* 2005; **38**(1):209–236.
36. Matthies HG, Keese A. Galerkin methods for linear and nonlinear elliptic stochastic partial differential equations. *Computer Methods in Applied Mechanics and Engineering* 2005; **194**:1295–1331.
37. Xiu D, Hesthaven JS. High-order collocation methods for differential equations with random inputs. *SIAM Journal on Scientific Computing* 2005; **27**(3):1118–1139.
38. Babuška I, Nobile F, Tempone R. A stochastic collocation method for elliptic partial differential equations with random input data. *SIAM Journal on Numerical Analysis* 2007; **45**(3):1005–1034.
39. Ganapathysubramanian B, Zabaras N. Sparse grid collocation schemes for stochastic natural convection problems. *Journal of Computational Physics* 2007; **225**(1):652–685.
40. Nobile F, Tempone R, Webster CG. A sparse grid stochastic collocation method for partial differential equations with random input data. *SIAM Journal on Numerical Analysis* 2008; **46**(5):2309–2345.
41. Nobile F, Tempone R, Webster CG. An anisotropic sparse grid stochastic collocation method for partial differential equations with random input data. *SIAM Journal on Numerical Analysis* 2008; **46**(5):2411–2442.
42. Phenix BD, Dinaro JL, Tatang MA, Tester JW, Howard JB, McRae GJ. Incorporation of parametric uncertainty into complex kinetic mechanisms: application to hydrogen oxidation in supercritical water. *Combustion and Flame* 1998; **112**:132–146.
43. Tatang MA. Direct incorporation of uncertainty in chemical and environmental engineering systems. *Ph.D. Thesis*, Massachusetts Institute of Technology, 1995.
44. Webster MD, Sokolov AP. A methodology for quantifying uncertainty in climate projections. *Climatic Change* 2000; **46**:417–446.
45. Reagan MT, Najm HN, Pébay PP, Knio OM, Ghanem RG. Quantifying uncertainty in chemical systems modeling. *International Journal of Chemical Kinetics* 2005; **37**(6):368–382.
46. Reagan MT, Najm HN, Debusschere BJ, Le Maître OP, Knio OM, Ghanem RG. Spectral stochastic uncertainty quantification in chemical systems. *Combustion Theory and Modeling* 2004; **8**:607–632.
47. Smith GP, Golden DM, Frenklach M, Moriarty NW, Eiteneer B, Goldenberg M, Bowman CT, Hanson RK, Song S, Gardiner Jr WC, Lissianski VV, Zhiwei Q. GRI mechanism for methane/air, version 3.0, 7/30/99. www.me.berkeley.edu/gri_mech.
48. Westbrook CK, Dryer FL. Simplified reaction mechanisms for the oxidation of hydrocarbon fuels in flames. *Combustion Science and Technology* 1981; **27**:31–43.
49. Hsu J, Mahalingam S. Performance of reduced reaction mechanisms in unsteady nonpremixed flame simulations. *Combustion Theory and Modelling* 2003; **7**:365–382.
50. Sivia DS. *Data Analysis*: *A Bayesian Tutorial*. Oxford: London, 1996.

DOI: 10.1002/nme

51. Jaynes ET. In *Probability Theory*: *The Logic of Science*, Bretthorst GL (ed.). Cambridge University Press: Cambridge, U.K., 2003.
52. Emery AF, Valenti E, Bardot D. Using Bayesian inference for parameter estimation when the system response and experimental conditions are measured with error and some variables are considered as nuisance variables. *Measurement Science and Technology* 2007; **18**(1):19–29.
53. Metropolis N, Rosenbluth AW, Rosenbluth MN, Teller AH, Teller E. Equations of state calculations by fast computing machines. *Journal of Chemical Physics* 1953; **21**(6):1087–1092.
54. Tierney L. Markov chains for exploring posterior distributions. *The Annals of Statistics* 1994; **22**(4):1701–1728.
55. Gilks WR, Richardson S, Spiegelhalter DJ. *Markov Chain Monte Carlo in Practice*. Chapman & Hall: London, 1996.
56. Haario H, Saksman E, Tamminen J. An adaptive metropolis algorithm. *Bernoulli* 2001; **7**:223–242.
57. Atchade YF, Rosenthal JS. On adaptive Markov chain Monte Carlo algorithms. *Bernoulli* 2005; **11**:815–828.
58. Janson S. *Gaussian Hilbert Spaces*. Cambridge University Press: Cambridge, U.K., 1997.
59. Debusschere BJ, Najm HN, Pébay PP, Knio OM, Ghanem RG, Le Maître OP. Numerical challenges in the use of polynomial chaos representations for stochastic processes. *SIAM Journal on Scientific Computing* 2004; **26**(2):698–719.
60. Brown PN, Byrne GD, Hindmarsh AC. Vode, a variable–coefficient ode solver. *Technical Report UCRL-98412*, Lawrence Livermore National Laboratory, Livermore, CA, June 1988; see also *SIAM Journal on Scientific and Statistical Computing* 1989; **10**:1038–1051.

DOI: 10.1002/nme